

Three-Dimensionality of Trajectories of Experimental Tracers in a Steady Axisymmetric Swirling Flow: Effect of Density Mismatch*

A.Yu. Gelfgat

Computational Mechanics Laboratory, Faculty of Mechanical Engineering, Technion,
Israel Institute of Technology, Haifa 32000, Israel
alexg@cmlp.technion.ac.il

Communicated by H.J.S. Fernando

Received 5 November 2001 and accepted 29 March 2002
Published online 2 October 2002 – © Springer-Verlag 2002

Abstract. The motion of tracer particles used for visualization in a steady axisymmetric swirling flow in a closed rotating disk–cylinder system is studied numerically. It is assumed that there exists a density mismatch between the particles and the fluid. It is shown that such a slight density mismatch leads to a deviation of the particle motion from steady axisymmetric streamlines, which in its turn yields non-axisymmetric patterns of the visualized flow. This gives a possible explanation for an existing disagreement between several experimental and numerical studies.

1. Introduction

The swirling flow in a closed rotating disk–cylinder system attracted the attention of many experimental and numerical studies during the two last decades (see [1–20] and references therein). The main objective of these studies was the vortex breakdown observed experimentally in this system and reproduced in various numerical studies. It was shown that the vortex breakdown appears and disappears as a continuous change of the flow topology and is not caused by an instability of the flow [9]. Recently, the main attention was drawn towards instabilities of the primary axisymmetric steady flow [9, 10] and further development of supercritical oscillatory flows that can be axisymmetric or three-dimensional [8, 11–20].

There exists a certain controversy related to the axisymmetry to non-axisymmetry (i.e., three-dimensional) transition of this flow, which occurs at relatively large Reynolds numbers. Following the conclusions of the experimental study [1] it is widely believed that at aspect ratios ($A = \text{height}/\text{radius}$) of the cylinder varying between approximately 1.5 and 3.5 the vortex breakdown is axisymmetric. This was supported by a number of axisymmetric calculations, e.g., [8] and [9], which reproduced the appearance and disappearance of the vortex breakdown for the same parameters as those observed in experiments [1]. Calculations with a sufficient accuracy were able to reproduce the experimentally observed size and position

* This research was supported by the Israel Science Foundation under Grant 240/01, by the Israel Ministry of Immigrant Absorption (to A. Gelfgat), the Israel High Performance Computer Unit, and by the Winograd Chair of Fluid Mechanics and Heat Transfer at Technion.

of the separation vortex bubble. Furthermore, a study of the topological bifurcations of the axisymmetric streamlines [14] also reproduced the experimental boundaries of the vortex breakdown. On the other hand, the authors of experimental study [11] argued that the patterns produced by tracers of visualization particles immersed in the flow are not axisymmetric and recalled that in all previous experiments done for this and similar configurations [1–7, 16, 21–23] the non-symmetry of such patterns is clearly seen. Figure 1 shows some such asymmetric experimental tracer patterns, reproduced from [1–4, 11, 22]. All the experimental photos are arranged so that the rotating disk is on the top of the cylinder. The asymmetry can be observed (i) inside of the vortex breakdown bubble (Figure 1(a),(b),(d)–(h)), (ii) as “streaks” coming out of the bubble in the downstream axial direction (Figure 1(a),(b),(d)–(g)), (iii) by spiraling streaklines observed in the axial cross-section of the cylinder (Figure 1(c)), and (iv) by non-symmetric tracer patterns in the axial cross-section taken very close to the rotating disk (not shown in Figure 1, see [11]). In [11] the non-symmetry of the tracer patterns was attributed to non-axisymmetry of the stationary flow which has the developed vortex breakdown structure. It was also argued that the separation vortex bubble is not closed, as follows from the axisymmetric models, but open, which creates the non-symmetric tracer “streaks” coming out of the bubble [11]. These findings were supported by three-dimensional numerical simulations [12, 13], where similar non-axisymmetric streaklines structures were calculated. In summary, the discussion in [11] and [12] questioned the validity of previous axisymmetric studies.

On the contrary, recent analysis of the stability of steady axisymmetric states with respect to three-dimensional perturbations [10] showed that the axisymmetric flows with vortex breakdown remain stable up to the transition to an oscillatory state. Moreover, the stability results of [10] indicate that for aspect ratios between 1.63 and 2.76 even the oscillatory instability is axisymmetric, thus confirming the early conclusions of [1]. The results of three-dimensional stability analysis [10] were recently validated by a series of fully three-dimensional time-dependent calculations [15, 17–19], as shown in Figure 2. Thus, the results of [18] confirmed that in the vicinity of $A = 1.6$ there is a switch between the three-dimensional mode $k = 2$ and

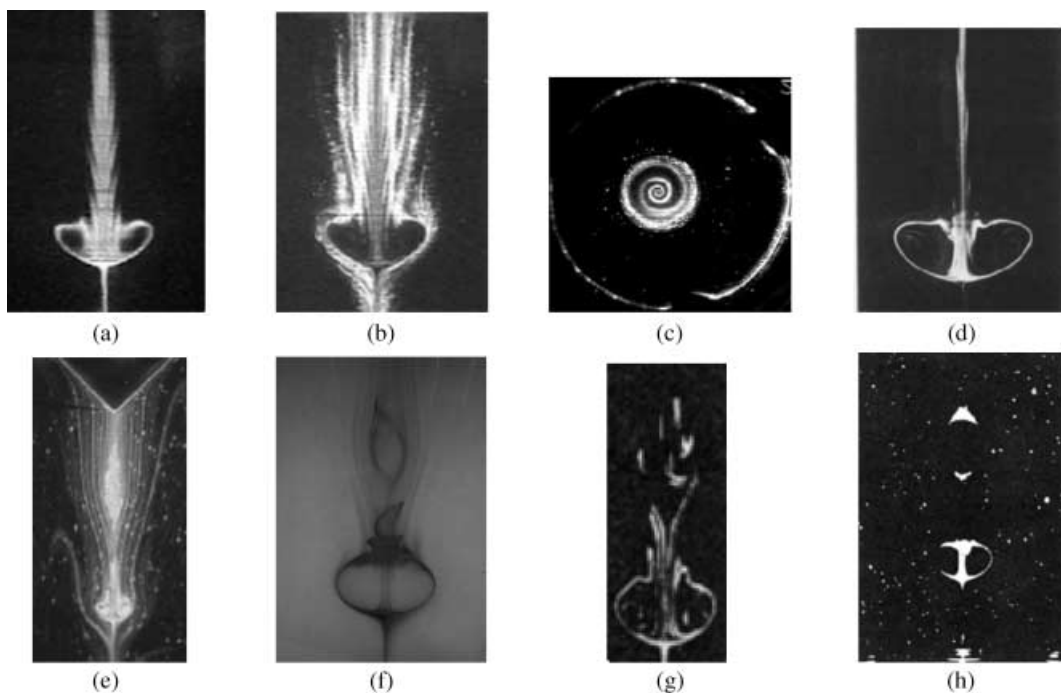


Figure 1. Experimental patterns of the streaklines. (a) [11], $\gamma = 1.75$, $Re = 1850$, visualization by fluorescent dye; (b),(c) [11], $\gamma = 1.75$, $Re = 1850$, visualization by electrolytic precipitation, meridional and axial cross-sections, respectively; (d) [1], $\gamma = 1.5$, $Re = 1747$, visualization by laser-induced fluorescence; (e) [22], $\gamma = 3$, $Re = 1655$, visualization by polystyrene particles; (f) [2], $\gamma = 2.24$, $Re = 2039$, visualization by K. Roesner (private communication); (g) [3], $\gamma = 2$, $Re = 2200$, visualization by fluorescent sodium dye; (h) [4], $\gamma = 2.5$, $Re = 2000$, visualization by small plastic spheres. Figure parts (a), (b), (c) and (e) are reproduced here with the kind permission of Cambridge University Press (resp. Figs. 4(a), 7(f) and 8(c) from [11] and Fig. 7(a) from [22]); part (f) was kindly supplied by Prof. K.G. Roesner; part (g) is reproduced here with the kind permission of ASME International.

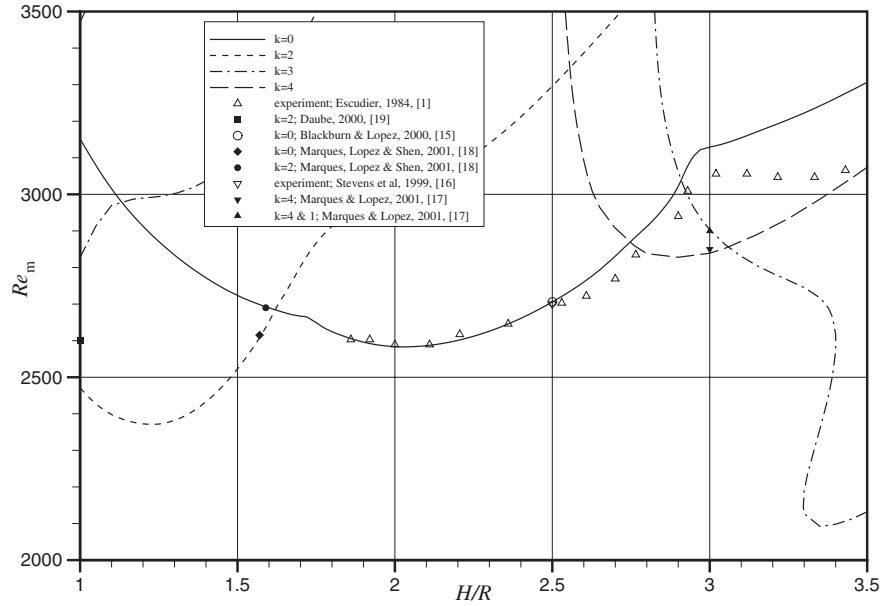


Figure 2. Diagram of the stability of the swirling flow in a cylinder with a rotating lid with respect to three-dimensional perturbations, and comparison with independent experimental and numerical data. k is the azimuthal wave number of a perturbation mode.

the axisymmetric mode $k = 0$ (here k is the azimuthal wave number of the three-dimensional perturbation mode), and the threshold to a three-dimensional flow with $k = 2$ was calculated in [19] for $A = 1$. The primary and secondary three-dimensional instabilities at $A = 3$ were calculated in [17]. This confirmed that the primary instability is caused by the mode $k = 4$, as was predicted in [10]. The secondary instability was found to occur with $k = 1$, causing the precession of the vortex breakdown bubble observed in [1]. Finally, the stability analysis [15] and experiments [16] confirm the axisymmetric steady–oscillatory transition at $A = 2.5$.

Furthermore, several experimental studies based on LDV measurements of the axial velocity along the cylinder axis [6, 21, 22] reported the existence of two stagnation points at the axis. This means that the separation vortex bubble is closed, contrary to the conclusion of [11] derived from observation of the streakline patterns. Moreover, a closer examination of the different experimental visualizations (Figure 1) reveals that the observed non-symmetric streakline patterns do not show much similarity for different experiments made for different governing parameters, as well as for experiments performed by the same authors for the same governing parameters but using different visualization techniques (see Figure 1(a),(b)). This allows one to assume that the observed streakline patterns depend not only on the flow studied, but also on the visualization technique used.

The present paper offers a possible explanation of the lack of similarity and of the controversial disagreement between the observed non-symmetric patterns of tracer particles, LDV measurements, numerical results reporting that the axisymmetric flow considered is stable for a wide range of parameters including those of experiment [11], and numerical simulation [12]. The lack of similarity is attributed to a mismatch between the densities of the experimental fluid and the visualization particles, which leads to the appearance of excessive buoyancy, centrifugal, and Coriolis forces. For example, in experiment [11] the density mismatch was reported to be 2%. To estimate this effect we assume that the experimental setup is perfectly axisymmetric, that the fluid flow is axisymmetric, and that the tracer particles remain on the streamlines of the *steady and axisymmetric* flow if the densities of the fluid and the particles are exactly same. If the densities of the fluid and the particles are slightly different the particles are affected by the buoyancy, centrifugal, and Coriolis forces, which are assumed to be balanced by the Stokes drag force. Therefore, only the drag force and the forces caused by the density mismatch are accounted for, while all other forces (e.g., inertia, pressure gradient, added mass, Basset and Faxen terms), that can lead to a deviation of a particle trajectory from the streamline it started from, are neglected. It is shown that the motion of such particles deviates

from the axisymmetric streamlines. The non-symmetric tracer patterns produced by these particles are qualitatively similar to those observed in the experiments. It is also shown that only when all three forces act together can a qualitative agreement with experimental observations be obtained. It is concluded finally that non-axisymmetric streaklines can be produced by steady axisymmetric swirling flows, so that no conclusion about flow three-dimensionality can be drawn on the basis of non-axisymmetric streakline patterns only.

2. Formulation of the Problem

We consider the motion of tracer particles driven by a *steady axisymmetric flow* $\mathbf{v} = (u(r, z), v(r, z), w(r, z))$ in a cylindrical coordinate system (r, φ, z) . The fluid is Newtonian with the density ρ_{fluid} and viscosity η . The most complete equations of motion for a spherical particle moving in a non-uniform unsteady flow at small Reynolds number are given in [24]. Here we also assume that the experimental tracer particles are spherical, but we use a much simpler model of their motion. To study the effect of the density mismatch we assume that the tracers will be “perfect” if $\rho_{\text{fluid}} = \rho_{\text{particle}}$. The term “perfect” means that a tracer will remain on a certain streamline (or an axisymmetric stream surface) of the *steady and axisymmetric* flow for an infinitely long time. Therefore, we neglect all the terms in the particle motion model [24], which can lead to any deviation of the “perfect” particle trajectory from the streamline it started from and, consequently, to a non-axisymmetric motion. It is also assumed that the disturbances of the fluid flow field introduced by the tracers are negligibly small, since otherwise the reliability of an experiment can be questioned. Following the arguments of [25] it is assumed that (i) all the tracer particles are spherical and of uniform radius a , (ii) the flow is slow enough so that the Stokes drag law is valid, (iii) the friction forces caused by particle rotation and inertial forces caused by a non-uniform particle motion can be neglected, and (iv) the Basset history term and the Faxen corrections can be neglected. Under these assumptions the main forces acting on the particle are the Stokes drag force, buoyancy, centrifugal, and Coriolis forces. The last three forces result from the density mismatch. We assume additionally that the particle motion is quasi-stationary and quasi-uniform, so that the buoyancy, centrifugal, and Coriolis forces are balanced by the Stokes drag force. Thus

$$\begin{aligned} 6\pi\eta a (\mathbf{v}_{\text{particle}} - \mathbf{v}_{\text{fluid}}) = & -\frac{4}{3}\pi a^3 g (\rho_{\text{particle}} - \rho_{\text{fluid}}) \mathbf{e}_z + \frac{4}{3}\pi a^3 (\rho_{\text{particle}} - \rho_{\text{fluid}}) \frac{v^2}{r} \mathbf{e}_r \\ & - \frac{4}{3}\pi a^3 (\rho_{\text{particle}} - \rho_{\text{fluid}}) \frac{vu}{r} \mathbf{e}_\varphi, \end{aligned} \quad (1)$$

where the left-hand side is the Stokes drag force and the three terms of the right-hand side are the buoyancy, centrifugal, and Coriolis forces, respectively. Equation (1) is an extension of the model used in [25] to explain some experimental observations of three-dimensional buoyancy convection. Note that according to (1) the velocities of fluid and particle are equal if $\rho_{\text{fluid}} = \rho_{\text{particle}}$, which means that the particle is “perfect”. The particle velocity is easily derived from (1) as

$$\mathbf{v}_{\text{particle}} = \mathbf{v}_{\text{fluid}} + \frac{2}{9} \frac{a^2}{\eta} (\rho_{\text{particle}} - \rho_{\text{fluid}}) \left[-g \mathbf{e}_z + \frac{v^2}{r} \mathbf{e}_r - \frac{vu}{r} \mathbf{e}_\varphi \right]. \quad (2)$$

Assuming that the variables are rendered dimensionless by the length, time and velocity scales L , T , and U , respectively, the non-dimensional form of (2) reads

$$\mathbf{v}_{\text{particle}} = \mathbf{v}_{\text{fluid}} - F_{\text{buoyancy}} \mathbf{e}_z + F_{\text{centrifugal}} \frac{v^2}{r} \mathbf{e}_r - F_{\text{coriolis}} \frac{vu}{r} \mathbf{e}_\varphi, \quad (3)$$

where

$$F_{\text{buoyancy}} = \frac{2}{9} \frac{a^2 g}{\eta U} (\rho_{\text{particle}} - \rho_{\text{fluid}}), \quad (4)$$

$$F_{\text{centrifugal}} = \frac{2}{9} \frac{a^2 U}{\eta L} (\rho_{\text{particle}} - \rho_{\text{fluid}}), \quad (5)$$

$$F_{\text{coriolis}} = \frac{2}{9} \frac{a^2 U}{\eta L} (\rho_{\text{particle}} - \rho_{\text{fluid}}). \quad (6)$$

Note that the dimensionless parameters $F_{\text{centrifugal}}$ and F_{coriolis} are equal. However, to investigate the effect of each force separately we prefer to keep different notations for them. Now, by writing (3) in terms of the coordinates of a particle (r, φ, z) we obtain to a system of equations describing the particle motion:

$$\begin{cases} \dot{r} = u + F_{\text{centrifugal}} \frac{v^2}{r}, \\ r\dot{\varphi} = v - F_{\text{coriolis}} \frac{vu}{r}, \\ \dot{z} = w - F_{\text{buoyancy}}. \end{cases} \quad (7)$$

The flow was calculated by the global Galerkin method [9], so that the numerical approximation of velocities is prescribed analytically by the Galerkin series over the whole flow domain. Therefore, no additional interpolation in space is needed for the numerical time integration of (7). To account for a possible stiffness of the ODE system (7), it was solved numerically using the Adams–Bashforth predictor–corrector algorithm with automatic choice of the time step and the order, using the LSODA code¹, with the numerical tolerance set to 10^{-6} . To ensure that the results are not dependent on the time step or the order of the method, the tolerance was varied between 10^{-5} and 10^{-7} , which did not introduce any noticeable difference in the tracer patterns reported below. To model the experimental photographs obtained in light sheets we follow the algorithm used in [8, 9] and plot only those points of the particle trajectories which cross the planes $\varphi = 0$ and $\varphi = \pi$. The obtained pattern of the particles trajectories can be interpreted as a Poincaré mapping. It was shown [8] that when the particles move together with the fluid, the corresponding Poincaré mappings reproduce the experimentally observed axisymmetric flows in steady and oscillatory regimes. It is stressed, however, that the Poincaré mappings and their fractal properties are not an objective of this study. Here we focus on the streaklines patterns, which are observed experimentally at relatively short times and can be modeled numerically by consideration of the motion of very few particles at relatively short time integration intervals.

3. Results

To model the particles motion we consider the axisymmetric flow in a rotating disk–cylinder system [1–20] calculated for the aspect ratio $\gamma = H/R = 1.75$ and Reynolds number $Re = \Omega R^2 \rho_{\text{fluid}} / \eta_{\text{fluid}} = 1850$. Here H is the height and R is the radius of the cylinder and Ω is the angular velocity of the rotating disk. The time, length, and velocity scales are $T = \Omega^{-1}$, $L = R$, and $U = \Omega R$, respectively. The values of γ and Re correspond to one of the experiments [11], where the axial symmetry of the flow was questioned. According to the results of [9], the maximal meridional velocities, as well as the azimuthal velocity far from the rotating disk, are of the order $10^{-1} \Omega R$. The size of the tracer particles in different experiments was of order 10^{-3} m or one to two orders of magnitude less (see Table 1). Therefore, for $R \sim 0.1$ m the particle Reynolds number, defined as $Re_p = v_{\text{fluid}} a \rho_{\text{fluid}} / \eta_{\text{fluid}}$, is of order $10^{-3} Re$ or less. For $Re \sim 10^3$ we can estimate that $Re_p \sim 1$ or less. This, in particular, justifies the use of the Stokes drag force expression in (1).

For the chosen scales, (4)–(7) can be rewritten as

$$F_{\text{buoyancy}} = \frac{2}{9} \frac{a^2 R g \rho_{\text{fluid}}}{\eta^2 Re} (\rho_{\text{particle}} - \rho_{\text{fluid}}), \quad (8)$$

$$F_{\text{centrifugal}} = \frac{2}{9} \frac{a^2 Re}{\rho_{\text{fluid}} R^2} (\rho_{\text{particle}} - \rho_{\text{fluid}}), \quad (9)$$

$$F_{\text{coriolis}} = \frac{2}{9} \frac{a^2 Re}{\rho_{\text{fluid}} R^2} (\rho_{\text{particle}} - \rho_{\text{fluid}}). \quad (10)$$

Note that with an increase of the Reynolds number the relative effect of the buoyancy force decreases while effect of the centrifugal and Coriolis forces increases. To estimate the relative effect of the buoyancy and centrifugal (Coriolis) forces we introduce a parameter α :

$$\alpha = \frac{F_{\text{buoyancy}}}{F_{\text{centrifugal}}} = \frac{R^3 \rho_{\text{fluid}}^2 g}{\eta^2 Re^2}. \quad (11)$$

¹ See <http://www.netlib.org/odepack/doc>.

Table 1. Estimation of the parameters α , F_{buoyancy} , and $F_{\text{centrifugal}}$.

Reference	a (m) $\times 10^3$	R (m) $\times 10^3$	ρ_{fluid} (kg m $^{-3}$)	η (Pa s)	$\alpha Re^2 \times 10^7$	$\rho_{\text{particle}}/\rho_{\text{fluid}}$	$F_{\text{buoyancy}}Re$	$F_{\text{centrifugal}}/Re \times 10^6$
[1]	0.01–0.5*	95	1151	0.00691	23.34	1.05*	0.6–30.	0.0026–6.5
[3, 4]	0.9	71	1200	0.05	0.202	1.04	75	37
[7]	0.01–0.5*	70	1198	0.044	0.249	1.05*	0.012–29.70	0.0048–12
[11]	0.4	45.65	1151	0.00691	2.589	1.02	0.282	0.011
[16]	0.01–0.5*	95	1151	0.00691	23.34	1.05*	0.6–30.	0.0026–6.5
[21], [22]	0.001–0.01	50	1200	0.05	0.0706	1.14*	7.2×10^{-5} – 7.2×10^{-3}	10^{-4} – 10^{-2}

* Taken from a source different from the original paper.

Note that this parameter does not depend on the size and density of tracer particles. The characteristic values of the parameters α , F_{buoyancy} , and $F_{\text{centrifugal}}$ ($= F_{\text{coriolis}}$) are estimated in Table 1 for the experiments [1, 3, 4, 7, 11, 16, 21], and [22]. Estimation of F_{buoyancy} and $F_{\text{centrifugal}}$ is problematic because the sizes of the tracer particles are not always reported. Thus, according to different published sources, the size of fluorescent particles varies within two orders of magnitude, which does not allow us to estimate parameters (8)–(10). The parameter α , which can be estimated rather precisely, also varies within two orders of magnitude for different experiments. For the following qualitative calculations we use mainly the data of experiments [1, 11, 16] and choose $\alpha = 10$. The values of F_{buoyancy} and $F_{\text{centrifugal}}$, for which we observe a strong deviation of the tracers trajectories from axisymmetric streamlines, lie inside the intervals reported in Table 1.

The axisymmetric flow pattern is shown in Figure 3. The secondary meridional flow consists of the main vortex and a weak additional vortex located near the axis. The appearance of the latter is known as a vortex breakdown phenomenon. This smaller vortex, which appears and disappears at certain values of the Reynolds number, is called the “separation vortex bubble” (for details see [1, 8, 9] and references therein).

The first series of calculations was done for three particles released at the points $(r, z) = (0.01, 0.36)$, $(0.1, 0.5)$, and $(0.4, 0.5)$, which are located inside the recirculation vortex bubble, on the boundary of the latter, and on the main meridional vortex, respectively. The dimensionless integration interval was set to 10 000, which corresponds to 8500 rotations of the lid in experiments [1] and [16], and 12 000 rotations in the experiment [11] (the time scale of one rotation lap is $2\pi R^2/\nu Re$). Such a long time is necessary because there are

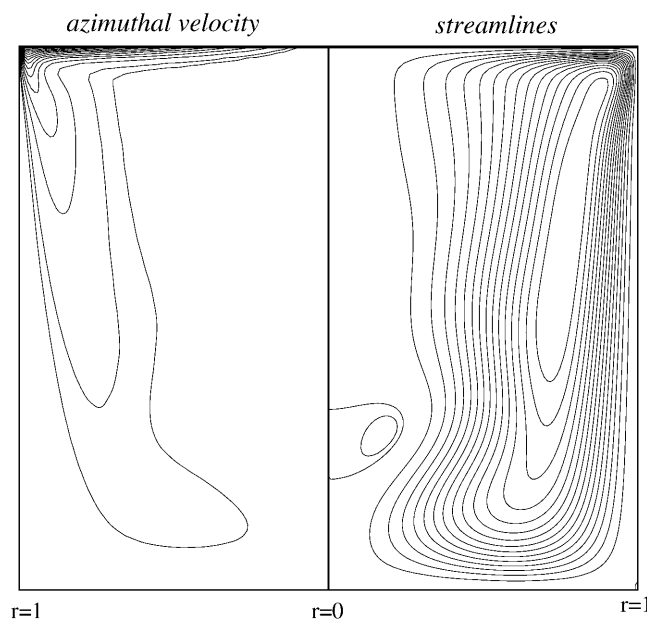


Figure 3. Streamlines of the meridional flow (right) and isolines of the azimuthal velocity (left) of the swirling flow in a cylinder with a rotating lid. $\gamma = 1.75$, $Re = 1850$.

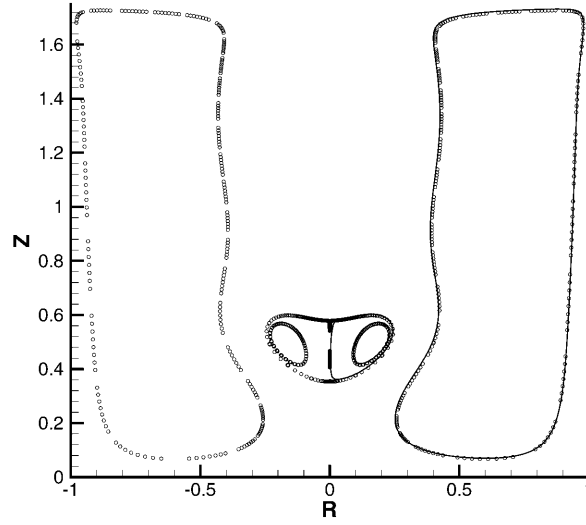


Figure 4. Patterns of three particle tracers for $\rho_{\text{fluid}} = \rho_{\text{particle}}$: all tracers are located on the streamlines. $F_{\text{buoyancy}} = F_{\text{centrifugal}} = F_{\text{coriolis}} = 0$. Starting points: \circ , (0.001, 0.36); Δ , (0.1, 0.5); \square , (0.4, 0.5).

too few particles in the present calculations compared with a laboratory experiment. Clearly, in the “perfect” case when $\rho_{\text{fluid}} = \rho_{\text{particle}}$, the tracers are always located on the streamlines. This is illustrated in Figure 4, which validates the numerical code. Subsequently, the goal is to study a possible deviation of the trajectories from the streamlines when the densities of fluid and particles do not match. By taking only one or two of the parameters F_{buoyancy} , F_{coriolis} , and $F_{\text{centrifugal}}$ to be non-zero, we examined the relative contribution of each force to the deviation of the trajectories.

When only the buoyancy force is accounted for (Figure 5) the tracers remain on closed lines, but deviate from the fluid streamlines. To explain this we consider $\mathbf{v}_{\text{particle}}$ in (3) as a spatially distributed function and notice that the continuity of $\mathbf{v}_{\text{fluid}}$ yields

$$\nabla \cdot \mathbf{v}_{\text{particle}} = \nabla \cdot \mathbf{v}_{\text{fluid}} - \nabla \cdot (F_{\text{buoyancy}} \mathbf{e}_z) = 0, \quad \text{when } F_{\text{coriolis}} = F_{\text{centrifugal}} = 0. \quad (12)$$

Note that F_{buoyancy} is not a function of the coordinates. Therefore we can define a “particle stream function” ψ_{particle} as $u_{\text{particle}} = (\partial \psi_{\text{particle}} / \partial z) / r$, $w_{\text{particle}} = -(\partial \psi_{\text{particle}} / \partial r) / r$, which is the integral of a particle

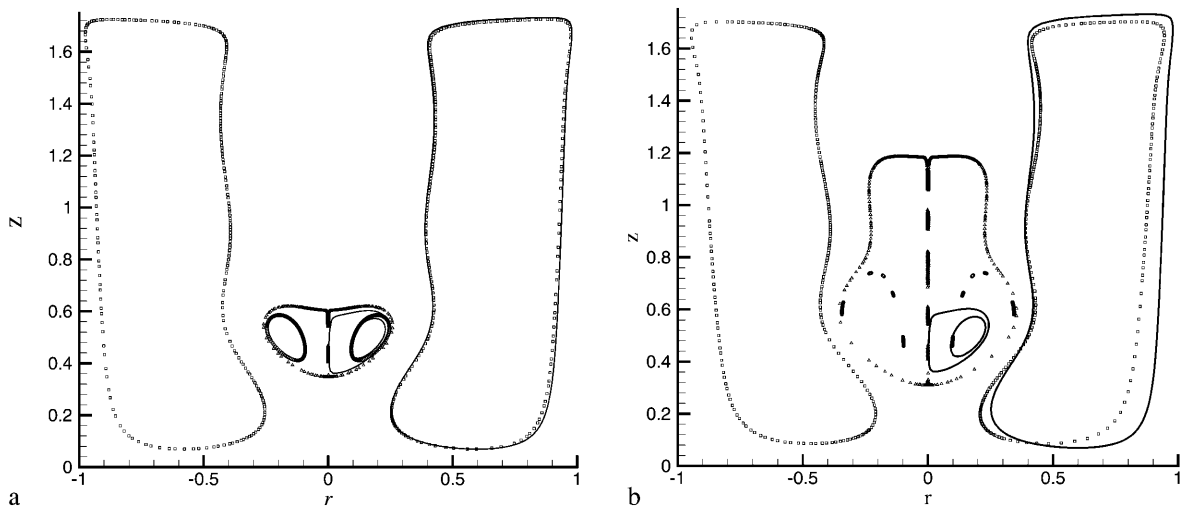


Figure 5. Patterns of three particle tracers affected by the buoyancy force only. $F_{\text{centrifugal}} = F_{\text{coriolis}} = 0$. Starting points as in Figure 3. (a) $F_{\text{buoyancy}} = 0.001$; (b) $F_{\text{buoyancy}} = 0.01$.

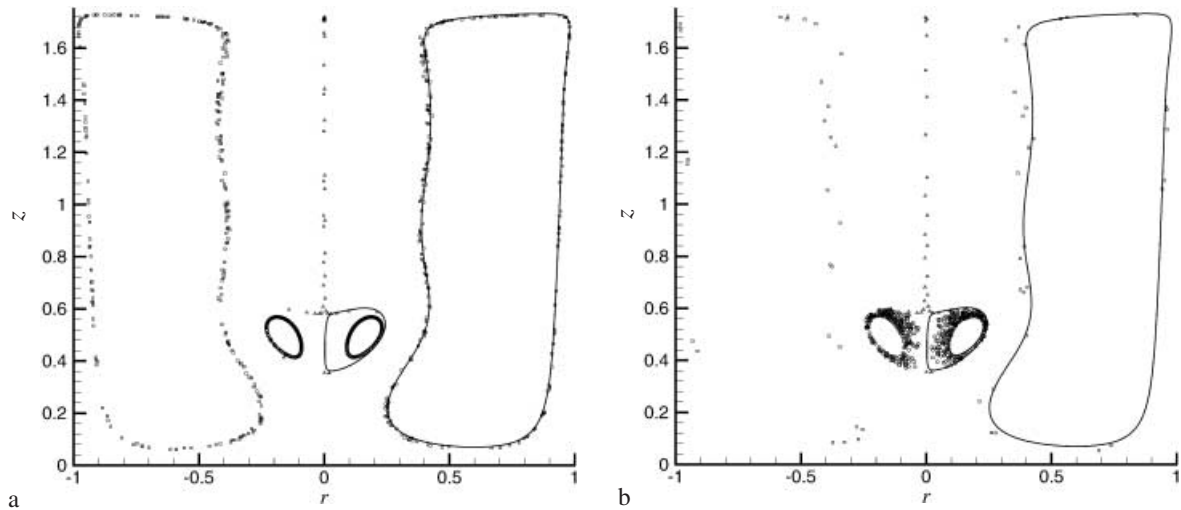


Figure 6. Patterns of three particle tracers affected by the centrifugal force only. $F_{\text{buoyancy}} = F_{\text{coriolis}} = 0$. Starting points as in Figure 3. (a) $F_{\text{centrifugal}} = 0.0001$; (b) $F_{\text{centrifugal}} = 0.003$.

motion. Obviously, the particle tracers will be located at the isolines $\psi_{\text{particle}} = \text{const.}$, similarly to the case of “perfect” particles (Figure 4). A large buoyancy force, i.e., larger density mismatch, apparently leads to a larger deviation of the tracers from the streamlines (see Figure 5). The observed effect is similar to the results of [26], where under certain conditions the trajectories of heavy particles driven by a spatially periodic vortex flow remained on closed lines. Obviously, these closed trajectories disappear at large density mismatches.

If only the centrifugal force is accounted for (Figure 6) the tracer patterns can be characterized by a smearing of the tracers around the fluid streamlines from which the motion of the particles started. This takes place at relatively small values of $F_{\text{centrifugal}}$ (small density mismatch) and at shorter times (Figure 6(a)). At longer times the particles leave the vortical core and reach the boundaries where their motion stops. The latter is already seen in Figure 6(a), where the particle initially located at the border of the separation vortex bubble reached the axis slightly above the axial stagnation point, and was then drawn upwards to the upper boundary. At larger $F_{\text{centrifugal}}$ (Figure 6(b)) the particle that started from the main meridional vortex reached one of the boundaries and stopped there. At the same time the particle that started from the inside of the separation vortex bubble remains there during all the integration time. However, the pattern of its streakline smears towards the border of the bubble and already cannot be interpreted as a line. Such smearing of the tracer pattern leads to the appearance of the Poincaré mapping points, which are located non-symmetrically. It is shown below that this asymmetry can be increased by the combined action of all three forces and can be mistakenly interpreted as an asymmetry of the flow as a whole.

The combined action of the buoyancy and centrifugal forces, assuming $F_{\text{coriolis}} = 0$, leads to a superposition of the previously described effects (Figure 7): (i) the tracer patterns smear around the lines which deviate from the streamlines and (ii) some of the tracers reach the boundaries and stop there. At the same time the combined action of the centrifugal and Coriolis forces, assuming $F_{\text{buoyancy}} = 0$, does not lead to any new features compared with the action of the centrifugal force only (see Figures 6 and 8).

The combined action of all three forces on the three particle tracers considered is shown in Figure 9. Obviously, a stronger smearing of all three tracers takes place. The smearing of the tracer that started from the streamline belonging to the main meridional vortex is significantly larger than that started from the separation vortex bubble. This seems to be a rather common experimental observation, i.e., the recirculation zones are usually visualized better than the main meridional vortex (e.g., Figure 1(e),(h)). At a stronger density mismatch (Figure 9(b)) the tracer that started from inside the separation vortex bubble produces a pattern, which can be interpreted, according to [11], as an “open bubble”. Note that no “open bubble” patterns were observed when the action of only one or two forces was considered.

To get a better insight into the appearance of possible non-symmetric tracer patterns it is necessary to consider more tracers (a “family” of particles) simultaneously. Thus, Figure 10 illustrates how a family of

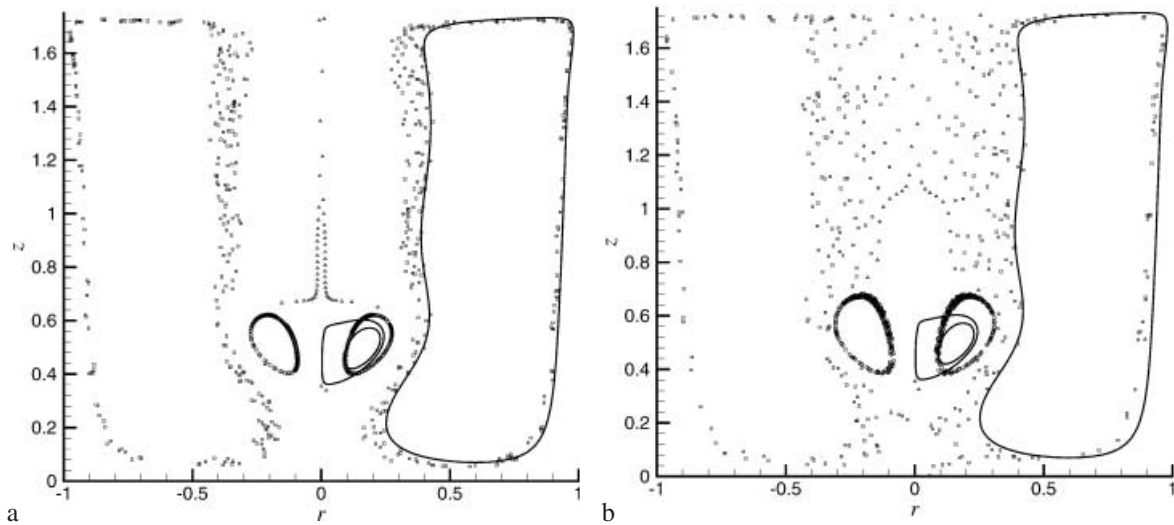


Figure 7. Patterns of three particle tracers not affected by the Coriolis force. $F_{\text{coriolis}} = 0$. Starting points as in Figure 3. (a) $F_{\text{buoyancy}} = 0.003$, $F_{\text{centrifugal}} = 0.0003$; (b) $F_{\text{buoyancy}} = 0.006$, $F_{\text{centrifugal}} = 0.0006$.

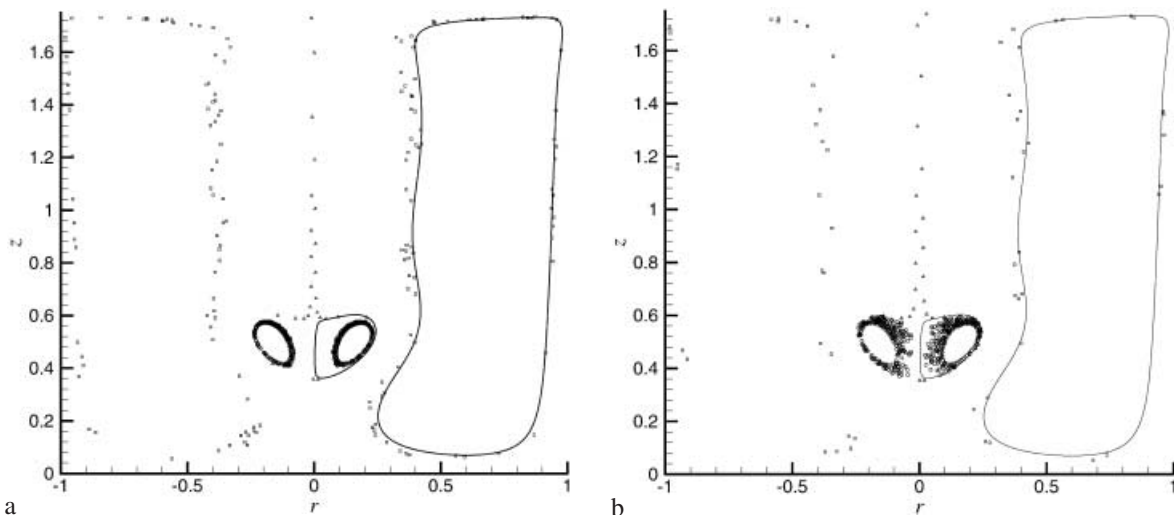


Figure 8. Patterns of three particle tracers not affected by the buoyancy force. $F_{\text{buoyancy}} = 0$. Starting points as in Figure 3. (a) $F_{\text{coriolis}} = F_{\text{centrifugal}} = 0.001$; (b) $F_{\text{coriolis}} = F_{\text{centrifugal}} = 0.003$.

particles that started inside the separation vortex bubble can lead to a non-symmetric tracer pattern. The non-symmetry persists for a rather long time. Thus, the patterns corresponding to the integration times of 500 and 1000 have qualitatively the same non-symmetry. Note that in several experimental photographs (Figure 1(a),(d),(e),(g),(h)) one side of the recirculation zone is “filled” by more tracers than the other one. At much longer times the whole area inside the pattern will be filled by the Poincaré mapping points, so that the pattern will look like an axisymmetric one.

Another family of particles released outside the separation vortex bubble (Figure 11) produces non-symmetric “streaks”, which were also observed in the experiments [1–3, 11, 16] and [22] (see also Figure 1(a),(b),(d)–(g)). The tracer pattern shown in Figure 11 illustrates that non-“perfect” particles deviate from the axisymmetric streamlines but they remain on certain lines forming the asymmetric “streaks”. These lines correspond to non-axisymmetric spiraling surfaces, which can be observed on the video-recorded experiments² (see also Figure 1(f)). These spiraling surfaces are observed as “streaks” in the meridional

² Private communication with Prof. K. Roesner. See also <http://fluids.me.usu.edu/VBDOWN/index.html>.

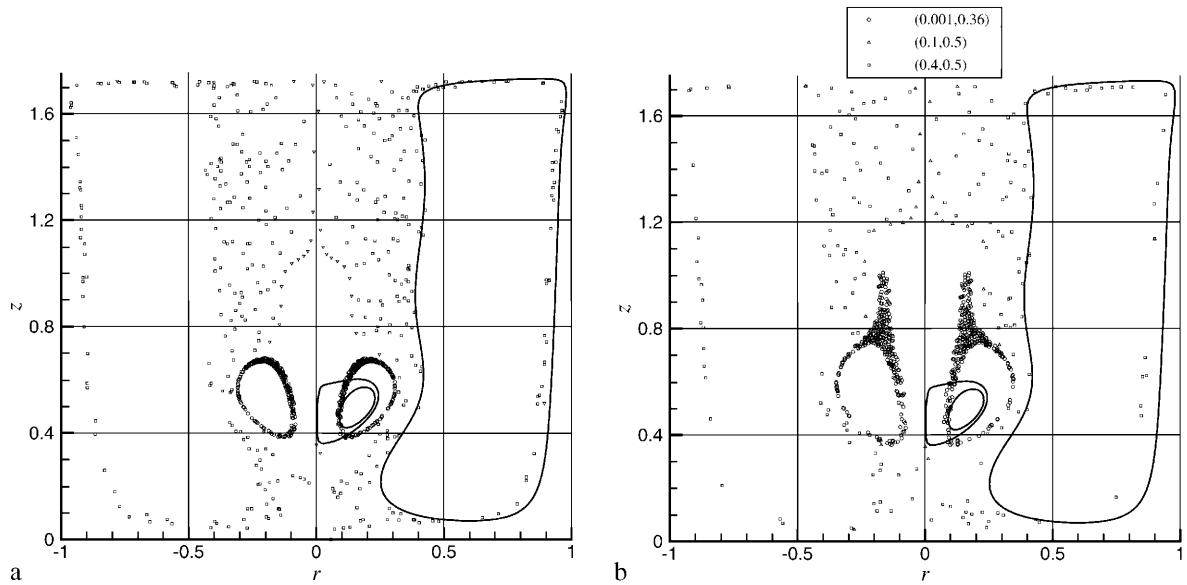


Figure 9. Patterns of three particle tracers affected by all forces. Starting points as in Figure 3. (a) $F_{\text{buoyancy}} = 0.006$, $F_{\text{coriolis}} = F_{\text{centrifugal}} = 0.0006$; (b) $F_{\text{buoyancy}} = 0.01$, $F_{\text{coriolis}} = F_{\text{centrifugal}} = 0.001$.

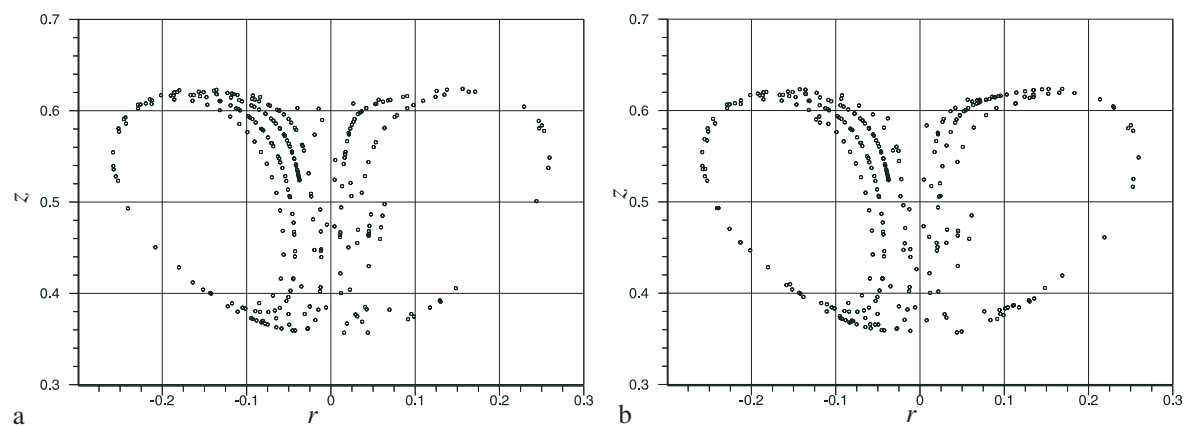


Figure 10. Patterns of tracers of a family of particles released from the rectangular $0.01 \leq r \leq 0.1$, $0.35 \leq z \leq 0.47$ with the steps of 0.001 and 0.1 in the r - and z -directions, respectively. $F_{\text{buoyancy}} = 0.001$, $F_{\text{coriolis}} = F_{\text{centrifugal}} = 0.0001$. (a) integration time 500; (b) integration time 1000.

cross-section, or as asymmetric spirals in the axial cross-section (Figure 1(c)). In [11] such spirals were attributed to the three-dimensionality of the flow, however, they can be produced also by an axisymmetric fluid motion. In spite of a long integration time of 10 000 all the particles reached the boundaries in a shorter time, which was approximately 1000.

Figure 12 illustrates the tracer patterns for families of particles released both inside and outside the separation vortex bubble. At shorter times one can observe both the non-symmetric pattern inside the bubble and the non-symmetric “streaks” (Figure 12(a)). When more particles are released and (or) the integration time is longer (Figure 12(b)) the Poincaré mapping points fill a certain symmetric area inside the bubble. However, the non-symmetric “streaks” remain in their places since, as mentioned above, the corresponding particles reach the no-slip boundaries and stop there. The calculated non-symmetric streaks are qualitatively similar to those observed experimentally (see Figures 12(b) and 1(b),(e)).

A closer look inside the symmetric patterns obtained during a long integration time and corresponding to the recirculation zones of the flow, is given in Figure 13. Clearly, if the integration time is long enough the tracer patterns look perfectly symmetric. However, a detailed look at the points shows that they are located

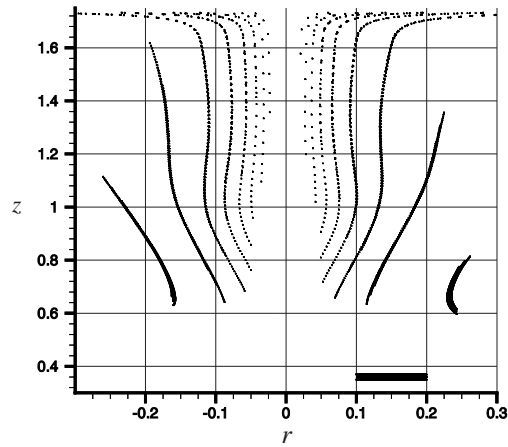


Figure 11. Patterns of tracers of a family of particles released from the interval $0.1 \leq r \leq 0.2$, with step of 0.001 at $z = 0.35, 0.36$, and 0.37. $F_{\text{buoyancy}} = 0.001$, $F_{\text{coriolis}} = F_{\text{centrifugal}} = 0.0001$.

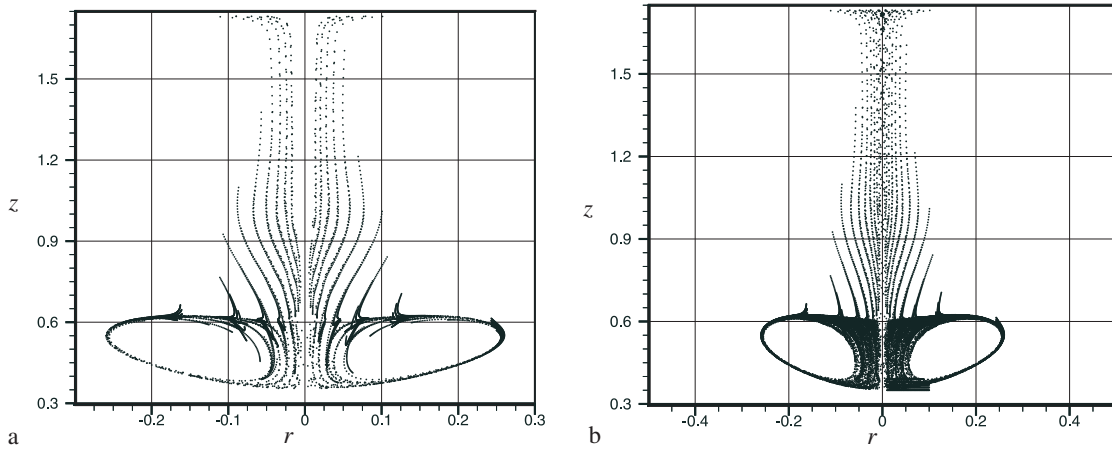


Figure 12. Patterns of tracers of a family of particles. $F_{\text{buoyancy}} = 0.001$, $F_{\text{coriolis}} = F_{\text{centrifugal}} = 0.0001$. (a) Released from the rectangular $0.01 \leq r \leq 0.1$, $0.35 \leq z \leq 0.4$ with the steps of 0.001 and 0.01 in the r - and z -directions, respectively; integration time 1000; (b) released from the rectangular $0.01 \leq r \leq 0.1$, $0.35 \leq z \leq 0.47$ with the steps of 0.001 and 0.01 in the r - and z -directions, respectively; integration time 10000.

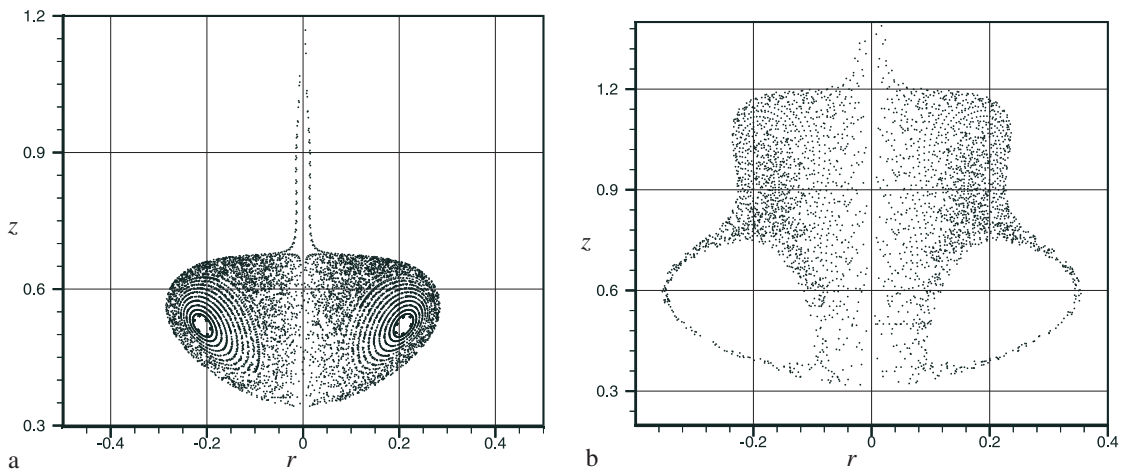


Figure 13. Patterns of tracers of a family of particles released from the interval $0.01 \leq r \leq 0.2$, with the step of 0.001 at $z = 0.5$. Integration time 10000. (a) $F_{\text{buoyancy}} = 0.003$, $F_{\text{coriolis}} = F_{\text{centrifugal}} = 0.0003$; (b) $F_{\text{buoyancy}} = 0.01$, $F_{\text{coriolis}} = F_{\text{centrifugal}} = 0.001$.

non-symmetrically. The same pattern can be observed if the number of tracer particles is large enough and the particles are released at properly distributed points. In other cases non-symmetric structures similar to those shown in Figures 10 and 12 can be observed.

4. Conclusions and Discussion

We have shown that under certain conditions tracers of non-“perfect” visualization particles (i.e., having a slight density mismatch with a working fluid) immersed in a *steady axisymmetric swirling flow* yield non-axisymmetric patterns. These non-axisymmetric patterns can be observed when (i) the number of particles is small, (ii) the observation time is relatively short, or (iii) the particles are released from certain localized areas. The experiments [11], which questioned the axisymmetry of the flow considered, reported a density mismatch of 2%. This could lead to the non-symmetric effects described here. The calculated trajectories reproduce a slight asymmetry inside the separation vortex bubble and the spiraling particle motion outside the bubble. This spiraling motion leads to the appearance of “streaks” in the meridional cross-section and to the spirals in the axial cross-section, both of which were observed in [11] and other experiments. Moreover, it was mentioned in [11] that the observed streakline patterns depend on the visualization technique and material (in particular, its density), e.g., are different for fluorescent dye and electrolytic precipitation techniques (Figure 1(a),(b)).

The present model for particle motion uses significant idealizations. Thus all the particles are assumed to be spherical and of uniform radius, which is apparently wrong for the dye used in the experiments [1, 16] and [11], but can be appropriate for the spherical polystyrene particles used in [19]. It is also not clear to what extent one can neglect the drag force caused by particle rotation, or the inertial and other forces caused by the non-uniform particles motion. It is not completely clear, as well, whether the Stokes drag law is applicable for the flows considered when the Reynolds number exceeds 1000. In fact, if the drag force were characterized by a term proportional to the squared velocity the described effects would only be stronger. However, in spite of all the idealizations made, the present modeling is capable of reproducing qualitatively the non-symmetric bubble patterns and non-symmetric “streaks” observed in all experiments. The tracer motion model used here cannot explain, for example, the non-axisymmetric tracer patterns observed in the axial cross-section close to the rotating disk. In this flow area the angular velocity is of the order ΩR at the disk and steeply decreases to zero at the stationary cylindrical wall. Therefore, the drag law should be reconsidered, the inertial effects cannot be neglected, and the particle motion cannot be considered as quasi-steady or quasi-uniform. Besides that, the particles released at a certain point at the sidewall are spun up by the flow, which can lead to local vortical instabilities. To model this experimental observations it will be necessary to consider the particle motion model of [24].

Note that when one of the forces was switched off the calculated patterns differed from the observed ones. Therefore, the observed effect is characteristic for axisymmetric swirling flows, i.e., when all three velocity components are non-zero axisymmetric functions and the fluid rotation is non-uniform. The appearance of asymmetric tracer patterns cannot be caused by density mismatch, in axisymmetric convective flows, in which the azimuthal velocity is zero or a constant.

Clearly, density mismatch is not the only source of experimental imperfections. The most common are small imperfections of axial symmetry, which always exist in the experimental setup. Such imperfections will alter the axial symmetry of the flow itself, and consequently will affect the three forces considered in the present study. One can speculate that a small change of the gravitational, centrifugal, and Coriolis forces, caused by geometrical imperfections, can lead to deviations of the tracer patterns from the expected axial symmetry qualitatively similar to those observed in the present study. Obviously, the combined effect of density mismatch and geometrical imperfections will only increase the non-symmetrical effects.

It should be noted that the effect of geometrical imperfections can be even stronger than expected. Thus, in experiments [2] and [23] the tracer particles were of molecular size. This means that the effect of the density mismatch considered was negligible (see (8)–(10)). However, a slight asymmetry in the patterns of vortex breakdown bubbles was observed and was attributed to the geometrical imperfections of the system. In the three-dimensional numerical study [12] and [13] the non-symmetric patterns of calculated streaklines were reported and were attributed to the asymmetry of the calculated steady flow. It was already argued, however, that a steady non-axisymmetry vortex breakdown bubble cannot exist in the non-uniformly rotat-

ing flow considered [20]. In the presence of the swirl the non-axisymmetric recirculation zone should rotate around the axis, as was reported by a series of recent three-dimensional calculations [17]–[19], as well as by the three-dimensional stability analysis [10]. The three-dimensional calculations of [12] used a non-uniform azimuthal mesh, which can be interpreted as a slight geometrical imperfection. It was already stated by the authors of [12] that the steady flow calculated on such a mesh has slight deviations from the axial symmetry, which, in turn, causes the asymmetric streakline patterns calculated on the basis of this flow. Furthermore, LDV measurements of the axial velocity along the cylinder axis [6, 21, 22] clearly revealed two stagnation points, thus indicating that the separation vortex bubble is closed. At the same time the non-symmetric tracer pattern, as well as the streaklines coming out of the bubble and propagating along the axis, was also seen in the experimental photographs reported in [21] and [22]. This direct velocity measurement shows that the topology of the bubble can be misinterpreted as an open one [11] if only tracer patterns are observed.

In the final conclusion we claim that the non-axisymmetric tracer patterns observed in the swirling flow considered should not necessarily be attributed to the three-dimensionality of the flow. It is shown here that the tracer patterns induced by a completely axisymmetric steady swirling flow can be non-axisymmetric if there is a small density mismatch between the particles and the working fluid.

References

- [1] Escudier, M.P. (1984). Observations of the flow produced in a cylindrical container by a rotating endwall. *Exper. Fluids* **2**, 189–196.
- [2] Roesner, K.G. (1990). Recirculation zones in a cylinder with rotating lid. In *Topological Fluid Mechanics* (H.K. Moffat and A. Tsinober, eds.), pp. 699–708. Cambridge University Press, Cambridge.
- [3] Fujimura, K., Koyama, H.S., and Hyun J.-M. (1997). Time-dependent vortex breakdown in a cylinder with rotating lid. *J. Fluids Eng.*, **119**, 450–453.
- [4] Uemura, T., Fujimura, K., Sung, H.-J., Hyun, J.-M., and Koyama, H. (1994). PTV measurement on a rotating system using semiconductor laser and ccd camera. *Proc. 7th Int. Symp. on Applications of Laser Technologies to Fluid Mechanics*, Lisbon, July 11–14, 1994, vol. II, pp. 22.3.1–22.3.6.
- [5] Böhme, G., Rubart, L., and Stenger, M. (1992). Vortex breakdown in shear-thinning liquids: experiment and numerical simulation. *J. Non-Newtonian Fluid Mech.*, **45**, 1–20.
- [6] Fujimura, K., Yoshizawa, H., Koyama, H.S., and Hyun, J.M. (2001). Velocity measurements of vortex breakdown in an enclosed cylinder. *J. Fluids Eng.*, **123**, 604–611.
- [7] Hourigan, K., Graham, L.J.W., and Thompson, M.C. (1995). Spiral streaklines in pre-vortex breakdown regions of axisymmetric swirling flows. *Phys. Fluids*, **7**, 3126–3129.
- [8] Lopez, J.M., and Perry A.D. (1992). Axisymmetric vortex breakdown. Part 3. Onset of periodic flow and chaotic advection. *J. Fluid Mech.*, **234**, 449–471.
- [9] Gelfgat, A.Yu., Bar-Yoseph, P.Z. and Solan, A. (1996). Stability of confined swirling flow with and without vortex breakdown. *J. Fluid Mech.*, **311**, 1–36.
- [10] Gelfgat A.Yu., Bar-Yoseph P.Z., and Solan A. (2001). Three-dimensional instability of axisymmetric flow in a rotating lid-cylinder container. *J. Fluid Mech.*, **438**, 363–377.
- [11] Spohn, A., Mory, M., and Hopfinger, E.J. (1998). Experiments on vortex breakdown in a confined flow generated by a rotating disk. *J. Fluid Mech.*, **370**, 73–99.
- [12] Sotiropoulos, F. and Ventikos, Y. (2001). The three-dimensional structure of confined swirling flows with vortex breakdown. *J. Fluid Mech.*, **426**, 155–175.
- [13] Sotiropoulos, F., Ventikos, Y., and Lackey, T.C. (2001). Chaotic advection in three-dimensional stationary vortex-breakdown bubbles: Sil’nikov’s chaos and the devil’s staircase. *J. Fluid Mech.*, **444**, 257–297.
- [14] Brøns, M., Voigt, L.K., and Sørensen, J.N. (1999). Streamline topology of steady axisymmetric vortex breakdown in a cylinder with co- and counter-rotating end-covers. *J. Fluid Mech.*, **401**, 275–292.
- [15] Blackburn, H.M., and Lopez, J.M. (2000). Symmetry breaking of the flow in a cylinder driven by a rotating endwall. *Phys. Fluids*, **11**, 2698–2701.
- [16] Stevens, J.L., Lopez J.M., and Cantwell B.J. (1999). Oscillatory flow states in an enclosed cylinder with a rotating endwall. *J. Fluid Mech.*, **389**, 101–118.
- [17] Marques F., and Lopez, J.M. (2001). Precessing vortex breakdown mode in an enclosed cylinder flow. *Phys. Fluids*, **13**, 1679–1682.
- [18] Marques F., Lopez, J.M., and Shen, J. (2002). Mode interactions in an enclosed swirling flow: A double Hopf bifurcation between azimuthal wavenumbers 0 and 2. *J. Fluid Mech.*, **455**, 263–281.
- [19] Daube, O. (2000). Private communication
- [20] Lopez, J.M., Marquez, F., and Sanchez, J. (2001). Oscillatory modes in an enclosed swirling flow. *J. Fluid Mech.*, **439**, 109–129.
- [21] Pereira, J.C.F. and Sousa, J.M.M. (1997). Steady and transient topologies of confined vortex breakdown generated by a rotating cone. *Opti. Diag. Eng.*, **2**, 61–70.

- [22] Pereira, J.C.F., and Sousa, J.M.M. (1999). Confined vortex breakdown generated by a rotating cone. *J. Fluid Mech.*, **385**, 287–323.
- [23] Bar-Yoseph, P.Z., Roesner, K.G., and Solan, A. (1992). Vortex breakdown in the polar region between rotating spheres. *Phys. Fluids A*, **4**, 1677–1686.
- [24] Maxey, M.R., and Riley, J.J. (1983). Equation of motion for a small rigid sphere in a nonuniform flow. *Phys. Fluids*, **26**, 883–889.
- [25] Yarin, A., Kowalewski, T.A., Hiller, W.J., and Koch, St. (1996). Distribution of particles suspended in convective flow in differentially heated cavity. *Phys. Fluids*, **8**, 1130–1140.
- [26] Tio, K.-K., Gañan-Calvo, A.M., and Lasheras, J.C. (1993). The dynamics of small, heavy, rigid spherical particles in a periodic Stuart vortex flow. *Phys. Fluids A*, **5**, 1679–1693.